

CHAPTER 132

NUMERICAL CALCULATION OF WAVE FORCES ON STRUCTURES*

B. D. Nichols and C. W. Hirt**

I. INTRODUCTION

A finite-difference technique for solving the Navier-Stokes equations for an incompressible fluid is used to calculate transient wave forces experienced by fixed and moving bodies. The numerical technique is based on the Marker-and-Cell (MAC) method developed by Harlow and Welch (1965). This new technique uses an especially simple solution algorithm that is designed for persons with little or no experience in numerical fluid dynamics. Originally conceived as an instructional tool, it has proven to be an extremely useful and versatile calculational method. Many useful calculations are possible with the publicly available code, SOLA-SURF, which is briefly described in Sec. II; however, the outstanding feature of this numerical scheme is the ease with which it can be modified to handle more complex problems. Reported here, in Sec. III, are examples to illustrate the utility of this new calculational tool for investigating the dynamic interactions between ocean waves and coastal structures.

II. THE NUMERICAL TECHNIQUE

The solution algorithm contained in SOLA-SURF solves the Navier-Stokes equations for an incompressible fluid. A stationary network of rectangular cells is used to divide the calculational region into a finite number of elements with which the fluid variables are associated. The primary field variables are the velocity components and the pressure. Each of the velocity components is specified at the center of the cell face to which it is normal and the pressure is specified at the cell center.

*This work was performed jointly under the auspices of the United States Energy Research and Development Administration and the Office of Naval Research, ONR Task #NR 062-455.

**The authors are members of the Fluid Dynamics Group (T-3), Theoretical Division, Los Alamos Scientific Laboratory, Los Alamos, NM 87545.

The fluid motion is numerically determined by advancing the fluid configuration through a series of small time increments. During each time step the solution to the momentum equation is obtained in two phases. First, the velocities and pressures from the previous time step are used to determine the fluid velocities in each cell, with the initial conditions used for the first time step. This explicit calculation does not necessarily ensure incompressibility; therefore, in the second phase the tentative velocity field is adjusted through changes in the pressure field. The pressure in each mesh cell is adjusted to drive to zero the velocity divergence in that cell. The pressure and velocity distributions must be obtained by iteratively adjusting these velocities in each cell in the mesh. This solution algorithm and other features of the technique are described in detail in a report by Hirt et al. (1975).

Free or curved rigid surfaces are permitted across the top and bottom of the computational mesh. The surfaces are defined by single valued functions of the height above the bottom of the computational mesh and are specified at the center of each vertical column of cells. The change in the free surface elevation is determined kinematically by the local fluid velocities, i.e., by the vertical component of the fluid motion plus the horizontal convection of the surface elevation from adjacent cell columns.

The free surface boundary conditions require that the normal and tangential velocities immediately outside the surface be chosen to ensure a zero transfer of momentum through the surface. A good approximation to these conditions is to set the velocities normal to the surface to satisfy the incompressibility condition in the cells in which the free surface is located and to set the tangential velocities in the cells immediately outside the fluid equal to the adjacent interior velocities. The pressure in surface cells is determined by a linear interpolation or extrapolation between the pressure in the fluid cell immediately below the surface cell and a specified pressure at the surface.

The pressure in each cell in which a rigid surface is located is derived under the constraint that the velocity normal to the surface be zero. This requires a variation in the Newton-Raphson type solution method used to obtain pressures for interior fluid cells. The velocity boundary conditions for these rigid boundaries are free-slip, i.e., the normal velocity and tangential velocity gradient are zero at the boundary, which makes them identical to the free surface boundary conditions. In addition, these rigid surface boundary conditions can be easily inserted in SOLA-SURF to create rigid, curved bodies at any location in the computational mesh. A special boundary condition section has been designated in the code to facilitate these types of modifications.

A copy of the SOLA-SURF code is available from the Argonne Code Center. The address is Argonne Code Center, Argonne National Laboratory, 9700 South Cass Avenue, Argonne, Illinois 60439.

III. THE CALCULATION OF WAVE FORCES ON STRUCTURES

We present four brief studies to illustrate the areas in which the ocean engineer may find SOLA-SURF to be a useful tool. The first two calculations, i.e., solitary wave run-up on a vertical wall and on a sloped beach, are good examples of what can be done with the relatively simple SOLA-SURF code without modification. The remaining calculations require the addition of special boundary conditions to create stationary or moving interior structures.

1. Reflection of a Solitary Wave

In this first example, a solitary wave travels over a fluid of constant depth, runs up a vertical wall, and reflects from the wall. The calculational region was resolved by 75 horizontal by 10 vertical cells, with cell dimensions of 0.5 horizontally and 0.2 vertically, and a time step of 0.1 was used. (The units in this calculation were non-dimensional.) All the wall boundaries were specified to be rigid, free-slip boundaries and the fluid is nearly inviscid. Laitone's second order approximation was used to initially define the free surface profile and velocity field of the solitary wave, as presented by Weigel (1964). The pressure field was initially set to hydrostatic pressure. Figure 1 shows the free surface profile and the velocity field, represented by velocity vectors drawn from cell centers, at times 13, 18, 20, and 26. The integrity of the wave profile and the velocity field remains excellent as the wave propagates down the channel and reflects from the wall.

To compare with the experiment of Camfield and Street (1967), the numerical calculation was repeated several times with initial wave heights ranging from 0.1 to 0.6, and with an undisturbed fluid depth of 1.0. A comparison of the computed maximum wave run-up with the experimental results is shown in Fig. 2. The abscissa is the ratio of the initial wave height, H_0 , to the undisturbed fluid depth, d , and the ordinate is the ratio of the maximum wave run-up on the vertical wall, R , to d . As the plot shows, the SOLA-SURF calculated data are in excellent agreement with these experimental data for a wide range of initial wave heights.

2. Solitary Wave on a Sloping Beach

Solitary waves are often used as the initial wave shape to simulate shoaling, breaking, and run-up of large, long waves on a beach. SOLA-SURF cannot handle breaking waves because of the restriction that the free surface slope be less than the mesh cell diagonal. This restriction can be removed by using the more complicated surface marker particle treatment as described, for example, by Nichols and Hirt (1971). However, we have calculated the solitary wave running up a sloped beach and measured the variation in maximum amplitude with depth. The rigid bottom slope was $1/20$, with the ratio of wave height to fluid depth of 0.1.

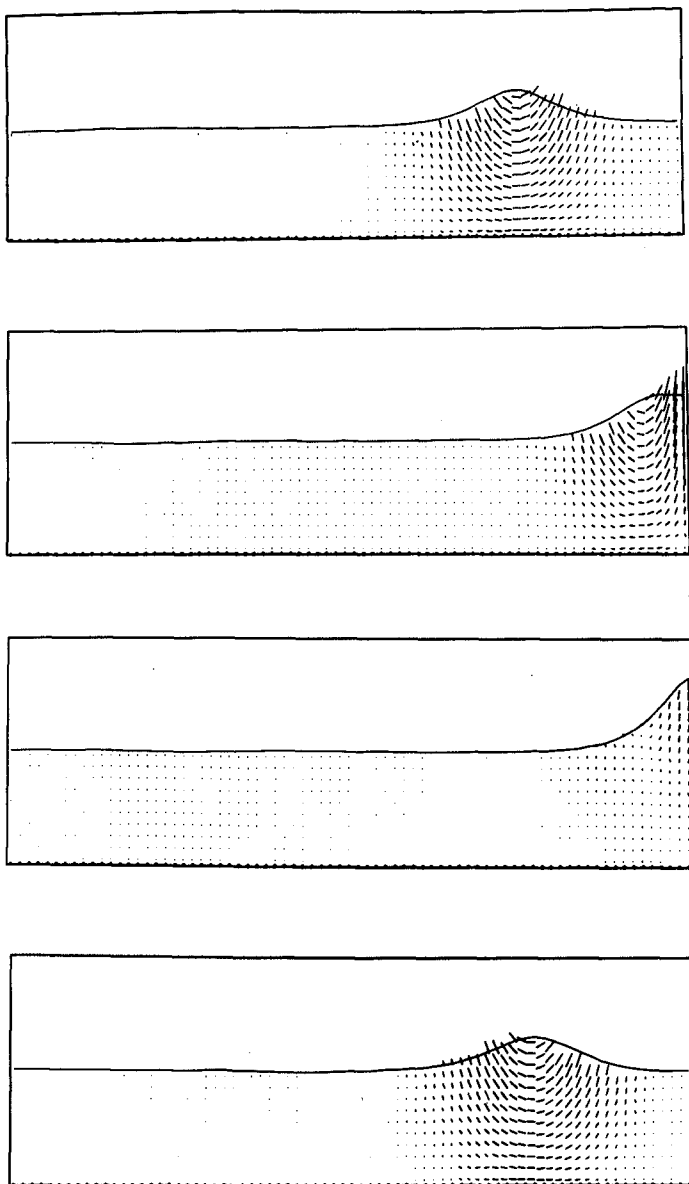


Fig. 1. Free surface profiles and velocity vector plots of solitary wave run-up on a vertical wall at times 13, 18, 20, and 26.

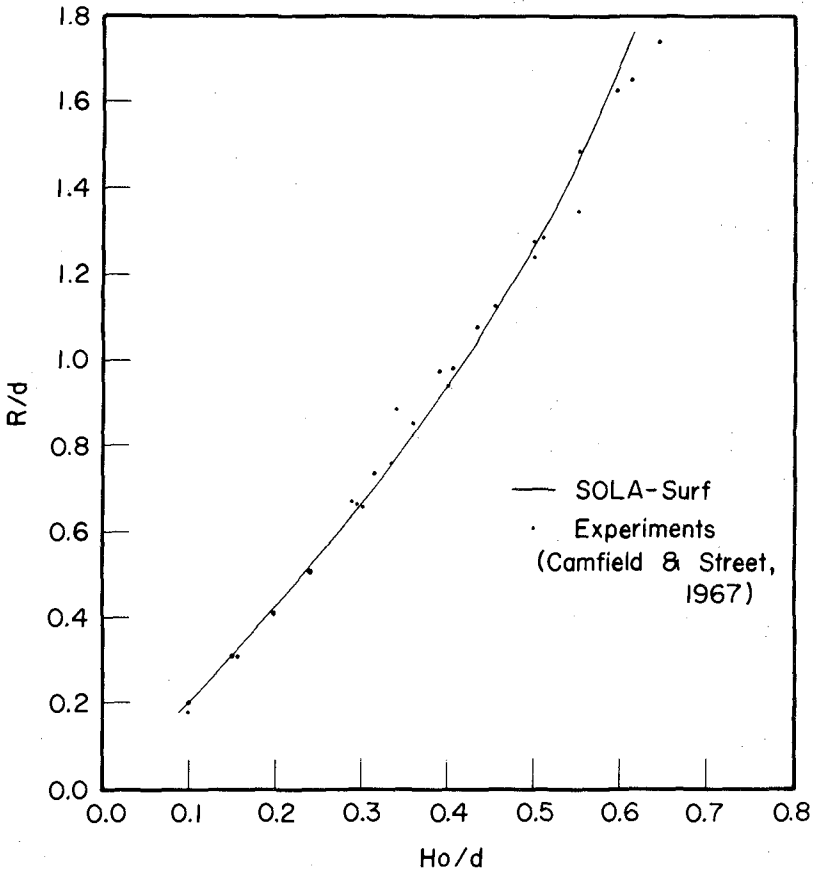


Fig. 2. A comparison of the computed maximum wave run-up, R , with experimental values for many initial wave heights, H_o .

Again, Laitone's second order approximation was used to initially define the solitary wave. Free-slip boundary conditions were specified for all rigid boundaries. A mesh of 90 horizontal by 18 vertical cells was used with cell dimensions of 0.5 horizontally and 0.1 vertically. The mesh length was chosen to accommodate the solitary wave totally over the horizontal section of the mesh bottom. SOLA-SURF does not have provisions to treat the intersection of the variable top and bottom boundaries in a cell. To allow the solitary wave to run farther up the beach without reflecting from the vertical wall, a shelf two and one-half cells beneath the undisturbed fluid surface was incorporated into the bottom boundary configuration. This is shown in Fig. 3, along with the free surface profile and the velocity field at times 0, 9, 22, and 28. At the later times, steepening of the wave front and growth of the wave height is obvious. Indeed, the calculated variation in maximum amplitude with depth compares very well with previous calculations, as shown in Fig. 4. In this plot, we compare the computed variation in maximum wave amplitude at different fluid depths with the theories of Peregrine (1967) and Madsen and Mei (1969). The numerical calculation of Chan and Street (1970) are virtually the same as the SOLA-SURF results. Peregrine derived equations of motion for long waves in water of varying depth that are extensions of the Boussinesq equations and that include nonlinear terms and a term to account for the effects of the vertical acceleration of the water on pressure. These equations were solved numerically for a solitary wave on a beach of uniform slope. Madsen and Mei treated the same problem with slightly different, but equivalent, equations. One difference, however, between the calculations is that Peregrine located the crest of the solitary wave immediately above the toe of the slope. The effect of this is seen in the comparison plot. Peregrine's calculation starts with $H/H_0 = 1.0$ at $d/d_0 = 1.0$, where H is the wave amplitude, H_0 is the initial wave amplitude, d is the undisturbed fluid depth at the horizontal location corresponding to the wave crest, and d_0 is the undisturbed fluid depth over the horizontal section of the bottom surface. The Madsen and Mei and SOLA-SURF calculations, which start with the wave initially over the flat bottom, show the ratio of the wave height at the toe of the slope to the initial wave height is greater than 1.0. The SOLA-SURF calculations are in good agreement with the other calculations. The effect of the shelf in our calculation is evident. The wave height does not continue to grow as the wave front reaches the shelf and, consequently, the value of H/H_0 falls slightly below values calculated without the shelf at low values of d/d_0 .

3. Forces on Submerged Structure

The determination of forces on submerged structures in the presence of gravity waves is of practical engineering importance. The SOLA-SURF code was used to calculate the horizontal and vertical forces on a submerged, rectangular structure resulting from a train of regular surface waves. This rectangular structure was created midway between the free surface and the mesh bottom by setting to zero the velocities on all faces of cells that make up the structure. These are set in the special boundary condition section of the code. The horizontal and vertical forces on the structure were determined by integrating the pressures acting on the surfaces of the structure. The dimensions of the submerged structure were chosen to compare with the experimental data of Brater et al. (1958).

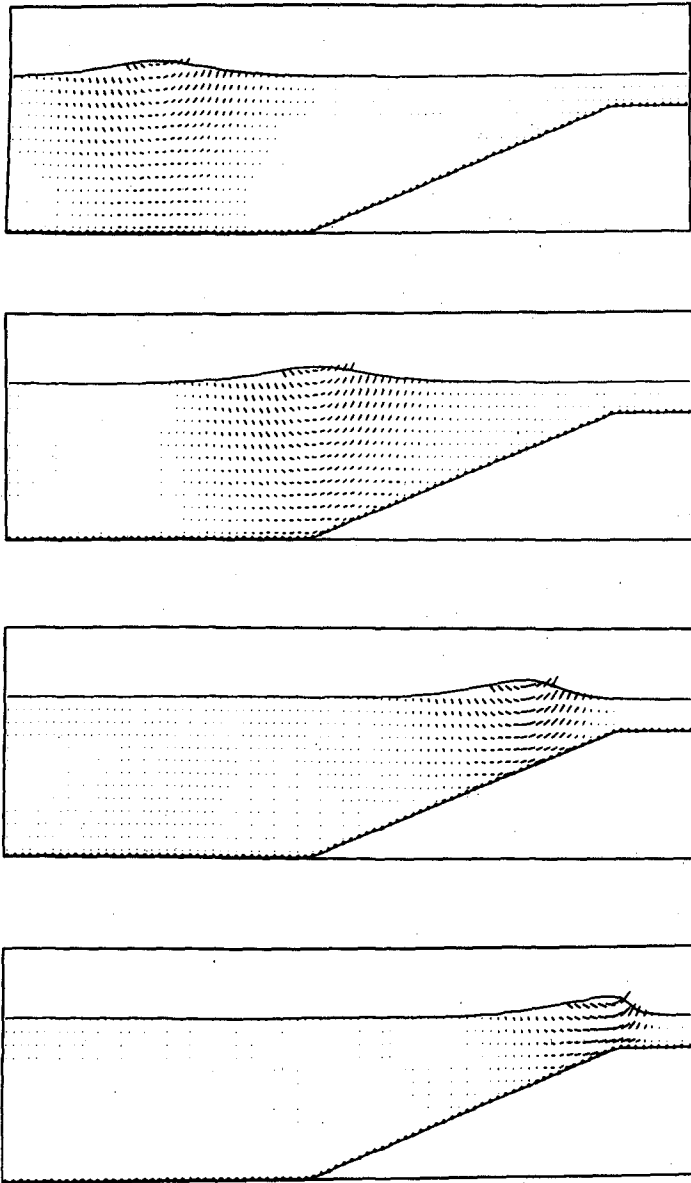


Fig. 3. Free surface profiles and velocity vector plots of solitary wave run-up on a 1/20 sloped beach at times 0, 9, 22, and 28.

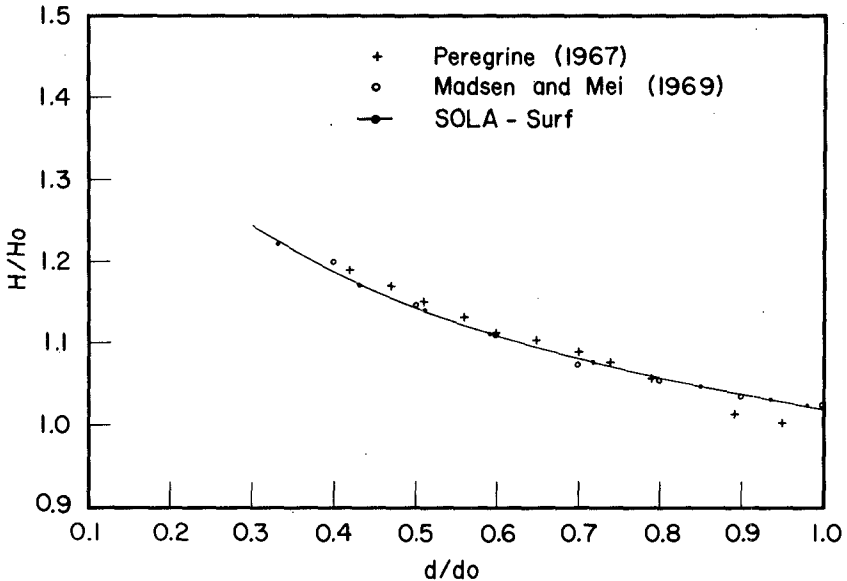


Fig. 4. A comparison of the computed variation in maximum wave amplitude, H , at different fluid depths, d , with other calculations.

The surface wave train was generated at the boundary of the computational mesh by setting the time dependent wave height and velocity components in the fictitious column of cells at the left side of the mesh. The mesh was 120 horizontal by 16 vertical cells, and the obstacle was 2 by 5 cells. Figure 5 shows the computer generated free surface profile, velocity field, and obstacle at times 0, 1.50, 3.25, and 4.25. The wave form is not perfectly sinusoidal; however, this is expected because an approximate shallow water expression was used to generate the wave form and, of course, the leading wave is distorted as it travels into still water. The exact form of the waves used in the experiment is not known.

Our computed data are compared with the experimental data in Fig. 6. The wave forces, normalized by wave height, are plotted as the vertical coordinate and the location of the center of the structure ($Y_b + d_o$), normalized by d_o , is plotted as the horizontal coordinate, where Y_b is zero at the free surface and d_o is the undisturbed fluid depth. The computed horizontal forces are in very good agreement with the experimentally determined forces of Brater et al. (1958). However, the

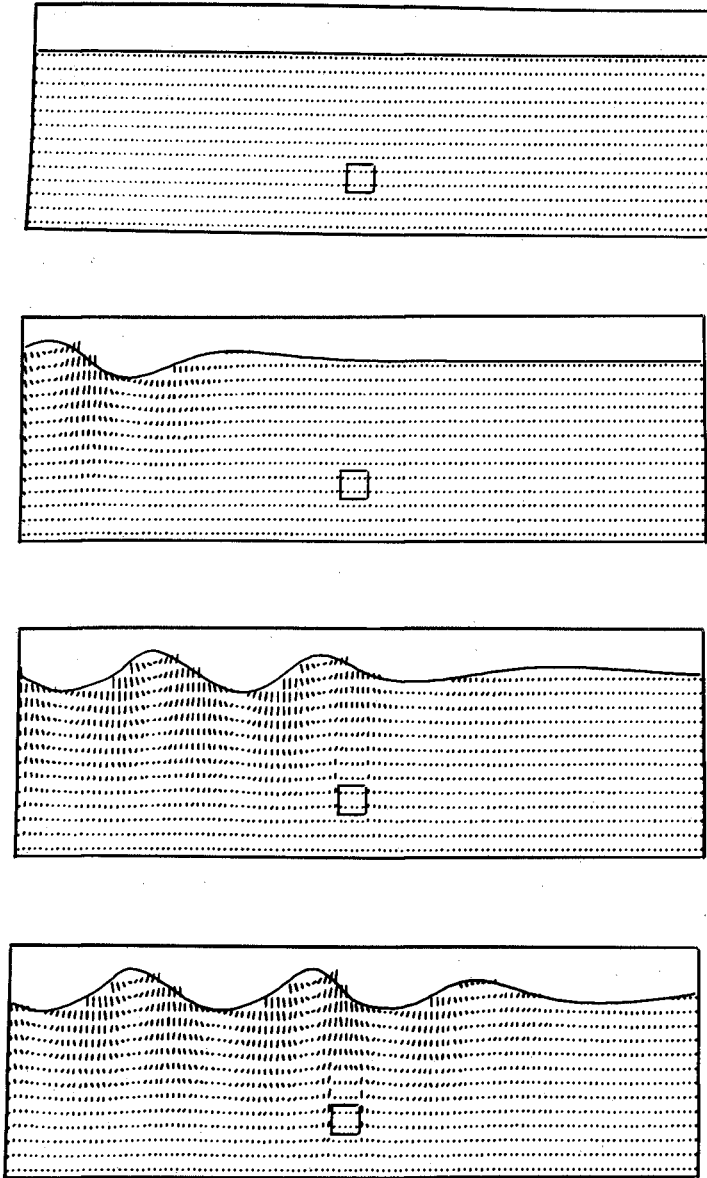


Fig. 5. Free surface profiles and velocity vector plots resulting from the propagation of a sinusoidal wave over a submerged structure at times 0, 1.50, 3.25, and 4.25.

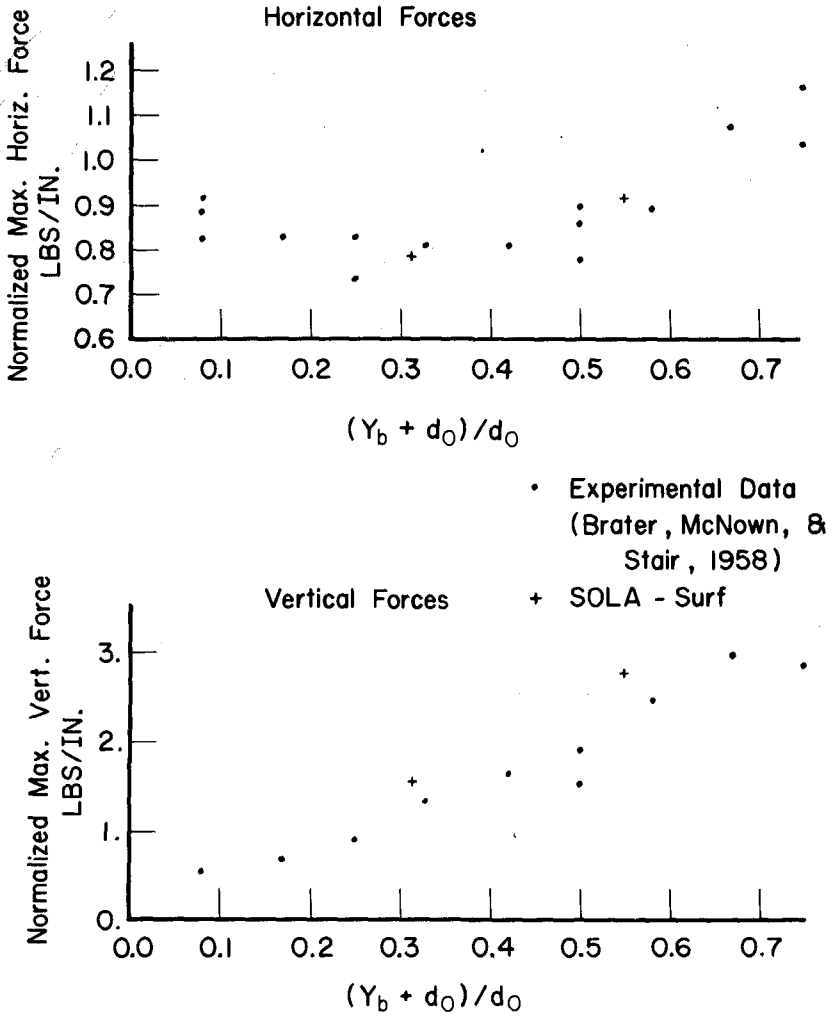


Fig. 6. A comparison of computed forces on a submerged structure with experimental data.

vertical forces calculated are about 20% larger than the experimental data. The accuracy of the numerical calculation was tested by increasing the temporal and spatial resolution and tightening the pressure iteration convergence criterion. These tests confirmed the originally calculated results, indicating that numerical accuracy is not the source of disagreement. Since the vertical force is very sensitive to the wave form, we may not be correctly modeling the experimental waves.

4. Forces on Floating Bodies

Hydrodynamic forces exerted on partially submerged, floating bodies are of interest to naval architects and ocean engineers. Different types of fluid motion may be generated to study these forces. Here we report on calculations for bodies undergoing forced harmonic oscillations in an otherwise quiescent fluid. In particular, we have studied heave forces on two-dimensional cylinders with rectangular and triangular cross sections and sway forces on a triangular or wedge shaped cylinder.

Pure heaving motions produce only vertical forces, which, for low amplitude motions, may be described by their amplitude and phase relative to the forced harmonic motion. These forces are due to buoyancy, inertial (added mass), and energy dissipation (wave generation) effects. In this study added mass and damping coefficients are computed and compared with the experimental work of Vugts (1968).

These calculations used mesh sizes that varied from 100 to 250 cells in the horizontal direction, depending on the period of motion, and 20 to 30 cells in the vertical direction. Typical calculation times on the CDC-7600 were 0.20 ms/cycle/cell. For the rectangular body, the mesh cell size was 0.1 horizontally and 0.2 vertically. Five cells were used to resolve the half-width of the body, which was located at a plane of symmetry at the left mesh boundary. Figure 7 shows the location of the rectangular body and the velocity field after approximately 2.5 periods of oscillation. To model the harmonic motion of the rectangular cylinder, special boundary conditions had to be added to the SOLA-SURF code. At the rigid bottom boundary of the rectangular body, the cell pressure is derived under the constraint that the normal fluid velocity be equal to that of the body. Because the SOLA-SURF boundary conditions restrict the surface slope to be less than that of a cell diagonal, we had to eliminate this restraint at the vertical side of the cylinder by aligning the side with a cell boundary line. Then boundary conditions were added to set zero velocities normal to the side of the cylinder.

The added mass coefficient, μ , and the damping coefficient, λ , are given by

$$\mu = \frac{\gamma \cos \beta}{\omega^2 a}$$

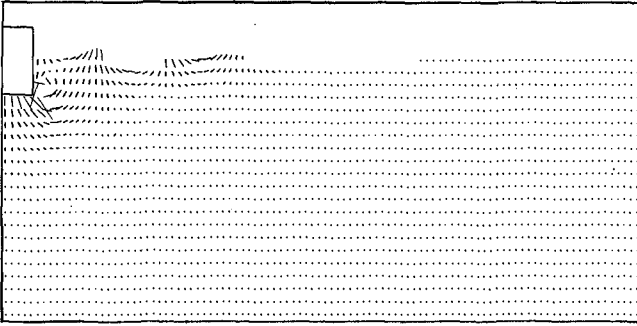


Fig. 7. Velocity vector plot of the fluid in which a rectangular cylinder is in forced heave at the left mesh boundary after 2.5 periods.

and

$$\lambda = \frac{\gamma \sin \beta}{\omega a} ,$$

where a is the amplitude of motion, ω is the frequency of motion, and γ is the amplitude of the assumed harmonic pressure force on the body. The phase shift β was obtained by comparing plots of the body displacement and pressure force acting on the rectangular body as functions of time and measuring the shift in phase. A detailed description of the determination of these coefficients is given by Nichols and Hirt (1975). These calculated added mass and damping coefficients are compared with experimental data in Fig. 8. The coefficients are normalized by ρA and $\sqrt{B/2g}$, where ρ is the fluid density, A is the mean submerged area, B is the rectangular body beam, and g is the acceleration of gravity. The calculations were for $B/T = 2.0$, where T is the rectangular body draft at its mean location. The amplitudes of motion, normalized by B , were 0.025 and 0.05. Vugts' experiments were conducted in fluid depths, normalized by B , varying from 4.50 to 5.625. The normalized depth was 4.0 for the calculated results. The calculated data generally agrees very well with the experimental data. The discrepancy in the calculated damping coefficient at the normalized frequency of 1.25 is probably due

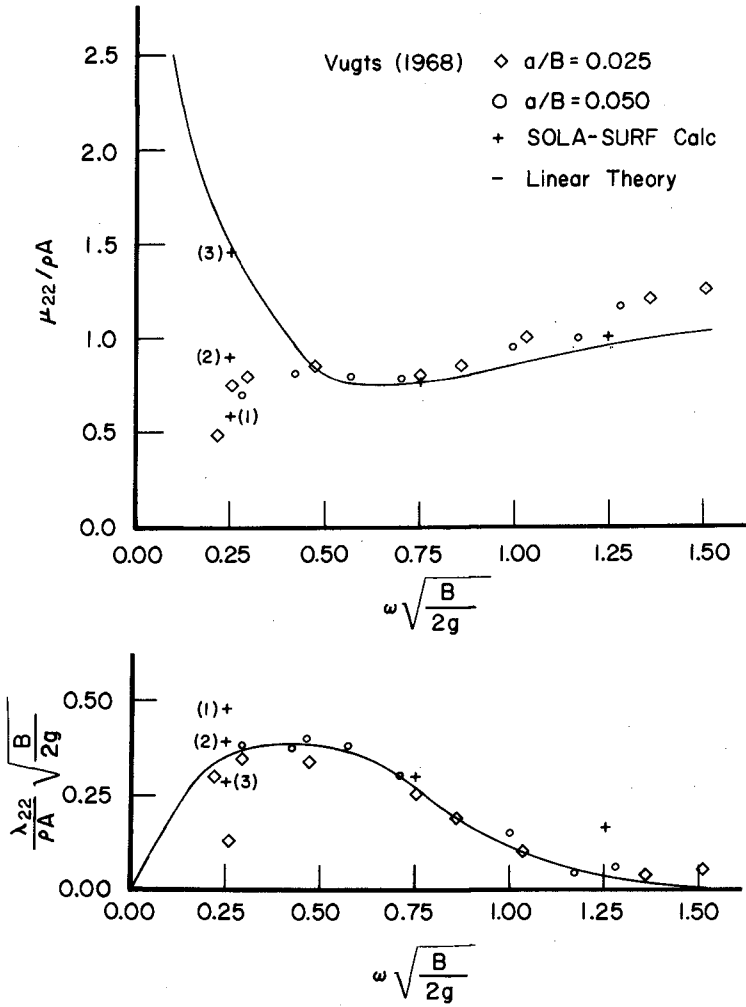


Fig. 8. A comparison of numerically computed and experimental values of added mass (top) and damping (bottom) coefficients from a rectangular cylinder in forced heave for $B/T = 2.0$.

to inaccuracies in determining the phase shift β , since it is very small at this beam width and frequency. To check this, another calculation was made, which is not plotted in Fig. 8, for $B/T = 8$ and $\omega\sqrt{B}/2g = 1.25$. In this case the phase shift is much larger, and the added mass coefficient agrees closely with the experimental data. The calculated damping coefficient in this case is very close to the experimental data, lying between the linear theory and the experimental data.

There is a discrepancy between the experimental data and linear theory for the added mass coefficient at normalized frequencies below 0.5. Vugts explains this as being caused by experimental inaccuracies. With a normalized fluid depth of 4.0, the calculated coefficient at a frequency of 0.25 is slightly higher than that of the experiments. (This is the middle point marked (2) in Fig. 8 at this frequency.) However, calculations with a fluid depth of 2.0, marked (1), and a fluid depth of 8.0, marked (3), show clearly that the finite depth is the cause of the disagreement with the linear theory. The added mass coefficient for the shallower fluid depth is slightly less than the experimental data, but with the normalized depth of 8.0 the calculated coefficient agrees with the linear theory, which assumes an infinite depth.

We next extended this capability to calculate the added mass and damping coefficients of a 60° wedge in sway. The coefficients, normalized as described above, were calculated for normalized frequencies ranging from 0.5 to 1.25 and with $B/T = 1.155$. An amplitude of motion, normalized by B , of 0.05773 was used. As shown in Fig. 9, the numerical data is in very good agreement with linear theory, but agrees less well with the experimental data. Expecting closer agreement with experimental data, we were concerned about possible numerical inaccuracies and tested for these in various ways. We tightened up the convergence criterion, increased by a factor of two the spatial and temporal resolution, used a new second order differencing scheme, and made various tests on the wedge interface boundary conditions. In addition, the calculations were performed in a moving reference frame attached to the body, as well as in the laboratory frame. However, all calculations were consistent to within a few per cent, thus, we believe the calculations are accurate.

Nonlinear effects were expected to have a greater influence. For example, secondary flow formed at the wedge tip is expected to increase the damping coefficient somewhat. This secondary vortex is shown in Fig. 10, which shows the velocity field and free surface configurations at times 0.50, 2.25, and 4.50. It should be noted that Vugts concluded that the generated eddy hardly disturbs the pressure distribution over the wedge surface. He explained the disagreement of his results with the linear theory as "a small systematic error at the higher frequencies of motion, where high demands are imposed on the structural set-up." We have shown that Vugts' tentative conclusions were correct and that linear theory does accurately predict the added mass and damping coefficients for the wedge in sway at this amplitude. Of course, at higher amplitudes for the forced sway, nonlinear effects must eventually enter.

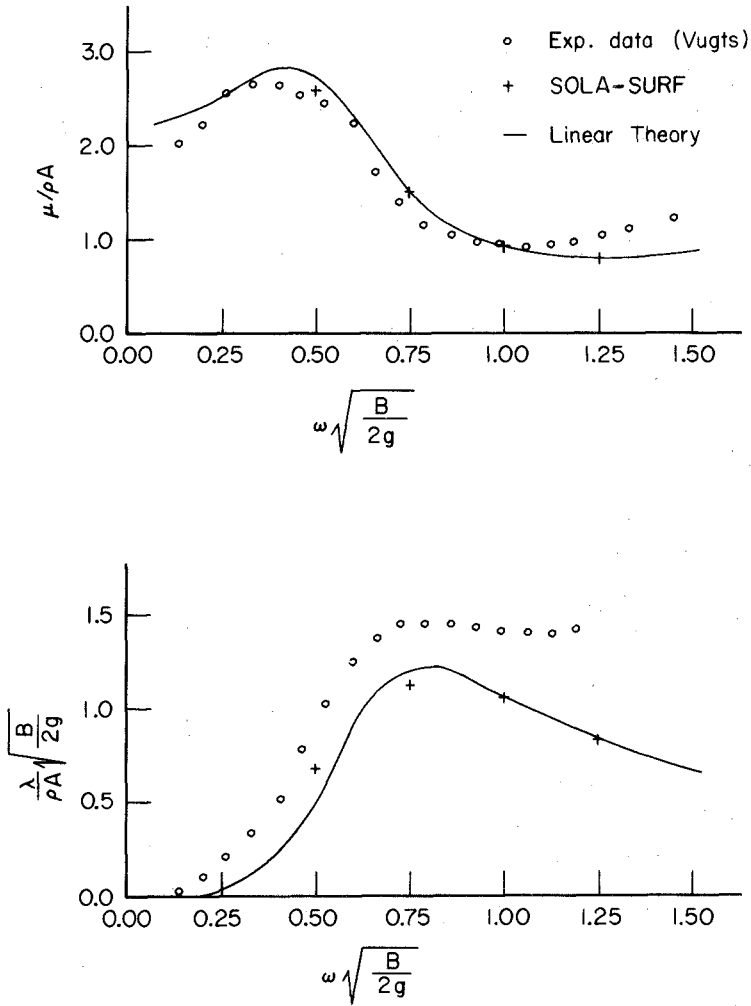


Fig. 9. A comparison of numerically computed and experimental values of added mass (top) and damping (bottom) coefficients from a 60° wedge in forced sway for $B/T = 1.155$.

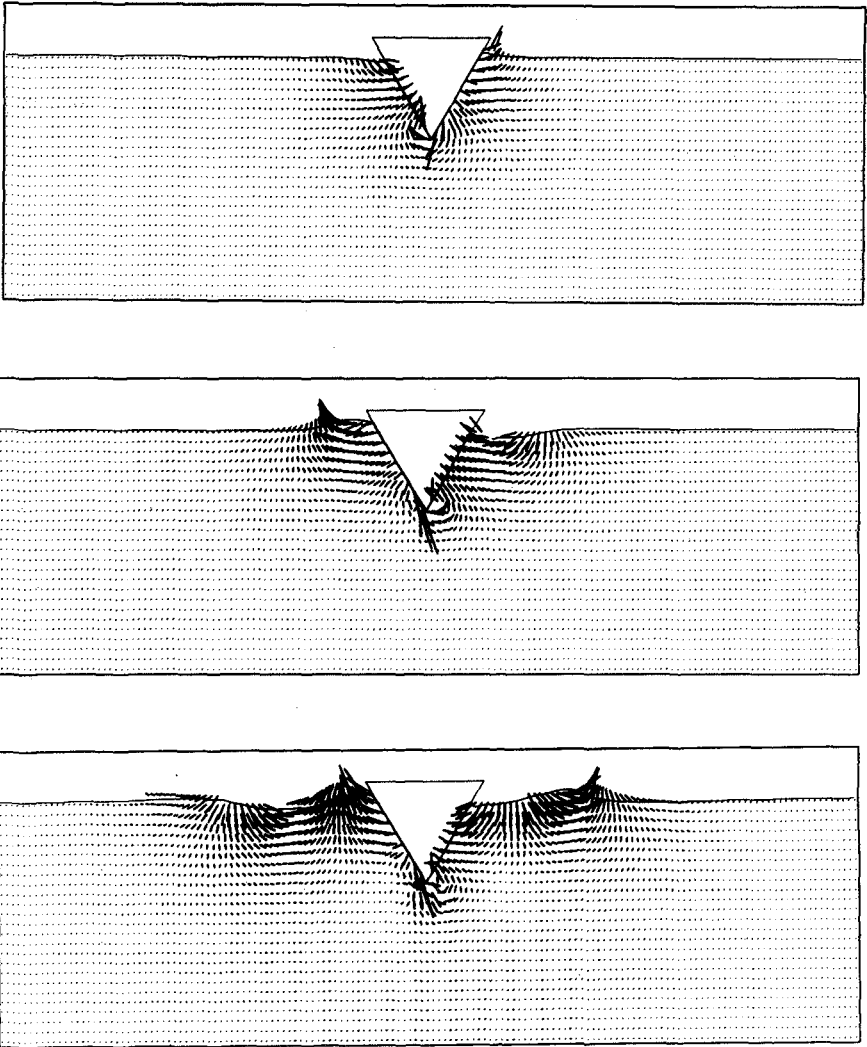


Fig. 10. Free surface profiles and velocity vector plots resulting from a 60° wedge in forced sway at times 0.50, 2.25, and 4.50.

REFERENCES

- Brater, E. F., McNow, J. S., and Stair, L. D., "Wave Forces on Submerged Structures," J. Hydraulics Division, ASCE, 84, Proc. paper 1833 (1958).
- Camfield, F. E. and Street, R. L., "An Investigation of the Deformation and Breaking of Solitary Waves," Stanford University Technical Report No. 81 (1967).
- Chan, R.K.-C. and Street, R. L., "SUMMAC - A Numerical Model for Water Waves," Stanford University Technical Report No. 135 (1970).
- Harlow, F. H. and Welch, J. E., "Numerical Calculation of Time-Dependent Viscous Incompressible Flow of Fluid with Free Surface," Phys. Fluids 8, 2182 (1965).
- Hirt, C. W., Nichols, B. D., and Romero, N. C., "SOLA - A Numerical Solution Algorithm for Transient Fluid Flows," Los Alamos Scientific Laboratory report LA-5852 (1975).
- Madsen, O. S. and Mei, C. C., "The Transformation of a Solitary Wave over an Uneven Bottom," J. Fluid Mech., 39, 781 (1969).
- Nichols, B. D. and Hirt, C. W., "Improved Free Surface Boundary Conditions for Numerical Incompressible-Flow Calculations," J. Comp. Phys., 8, 434 (1971).
- Nichols, B. D. and Hirt, C. W., "Methods for Calculating Multi-Dimensional, Transient Free Surface Flows Past Bodies," Proceedings of the First International Conference on Numerical Ship Hydrodynamics, Gaithersburg, MD (1975).
- Peregrine, D. H., "Long Waves on a Beach," J. Fluid Mech., 27, 815 (1967).
- Vugts, J. H., "The Hydrodynamic Coefficients for Swaying, Heaving, and Rolling Cylinders in a Free Surface," International Shipbuilding Progress, 15, 251 (1968).
- Wiegel, R. L., Oceanographical Engineering, Prentice Hall, Englewood Cliffs, New Jersey (1964).